Effect of tapered-end shape of FRP sheets on stress concentration in strengthened beams under thermal load

Benaoumeur El Mahi [1], Kouider Halim Benrahou [1], Sofiane Amziane [2],
Khalil Belakhdar [1], Abdelouahed Tounsi [*1] and El Abbes Adda Bedia [1]

[1] *Material and Hydrology Laboratory, University of Sidi Bel Abbes, Faculty of Technology,*
Civil Engineering Department, Algeria
[2] *Clermont University, Institut Pascal, Polytech'Clermont-Ferrand, 63174 Aubière Cedex, France*

Abstract. Repairing and strengthening structural members by bonding composite materials have received a considerable attention in recent years. The major problem when using bonded FRP or steel plates to strengthen existing structures is the high interfacial stresses that may be built up near the plate ends which lead to premature failure of the structure. As a result, many researchers have developed several analytical methods to predict the interface performance of bonded repairs under various types of loading. In this paper, a numerical solution using finite – difference method (FDM) is used to calculate the interfacial stress distribution in beams strengthened with FRP plate having a tapered ends under thermal loading. Different thinning profiles are investigated since the later can significantly reduce the stress concentration. In the present theoretical analysis, the adherend shear deformations are taken into account by assuming a parabolic shear stress through the thickness of both beam and bonded plate. The shear correction factor for I-section beams is also included in the solution. Numerical results from the present analysis are presented to demonstrate the advantages of use the tapers in design of strengthened beams.

Keywords: plate bonding; FRP composite; interfacial stresses; repaired beam; taper

1. Introduction

Extensive research and development, over the past decades, in the field of materials engineering and science have been carried out with fibre-reinforced plastic (FRP) composites leading to a wide range of practical applications (Seible *et al*. 1997, Mo *et al*. 1998, Li and Ghebreyesus 2006, Panjehpour *et al*. 2011) as a nation's infrastructure ages, one of the major challenges the construction industry faces is that the number of deficient structures continues to grow. The applications of using externally bonded FRP plates to reinforced concrete (RC) or steel structures have shown that the technique is effective, efficient and offers a practical solution to this pressing problem. Retrofitting using externally bonded plates is quick, easy with respect to material handling, causes minimal site disruption and produces only little changes in section size. In recent years, many studies have been carried out on the behaviour and strength of such

---

∗Corresponding author, Professor, E-mail: tou_abdel@yahoo.com

retrofitting method (Roberts 1989, Malek *et al*. 1998, Smith and Teng 2001, Pesic and Pilakoutas 2005, Stratford and Cadei 2006, Benyoucef *et al*. 2006, Tounsi and Benyoucef 2007, Yuan and Lin 2009, Yang *et al*. 2009, Zhu and Zhang 2010, Yang and Ye 2010, Hao *et al*. 2012, Krour *et al*. 2013). However, the disadvantage of this technique is that the strengthened members are susceptible to stresses concentration near the plate end, which may cause a total debonding between the member and the FRP plate. In additions, some experimental studies have revealed that the debonding failure is a common case of brittle failure in the strengthened beams with plate (Jones *et al*. 1988, Swamy *et al*. 1989, Oehlers 1992, Arslan *et al*. 2008). As a result, some researchers noted that reducing the FRP or steel plate thickness near the plate end is an effective method to minimize the interfacial stresses (Stratford and Cadei 2006, Gao *et al*. 2006a, b, c, Belakhdar *et al*. 2011).

As a further development of the solutions by Stratford and Cadei (2006), Smith and Teng (2001), Deng *et al*. (2004), Tounsi (2006) and Belakhdar *et al*. (2010), this paper presents a simple numerical solution for obtaining the shear and the normal stresses in the adhesive layer of a retrofitted beam under thermal loads. The method can be used to design strengthened beams with section properties that change along the beam such as tapered plates. Finally, a parametric study was conducted to compare the results of models with different geometries.

2. Theoretical formulation

2.1 Basic assumptions

The following assumptions were made in the analytical study:

- All materials considered as linear elastic.
- The beam is simply supported and shallow, i.e., plane sections remain plane in bending.
- No slip is allowed at the interface of the bond (i.e., there is a perfect bond at the adhesive steel or FRP plate interface).
- Bending deformations of the adhesive are neglected.
- Stresses in the adhesive layer do not change with the thickness.
- The shear stress analysis assumes that the curvatures in the beam and plate are equal (since this allows the shear stress and peel stress equations to be uncoupled).
- A parabolic shear stress distribution through the depth of both the beam and the bonded plate is assumed.

In case of reinforced concrete beams, the section properties were based on the uncracked section, excluding the convention al steel reinforcement.

2.2 Shear stress distribution along the FRP–beam interface

The present stresses derivations are mainly based on Tounsi *et al*. (2009) method. However, the final governing differential equations are solved using finite difference method in order to avoid complex solution in case of tapered plates.

A differential section, *dx*, can be cut out from the FRP-strengthened beam as shown in Figs. 1 and 2. The strains in the beam near the adhesive interface and the external FRP reinforcement can be expressed, respectively as
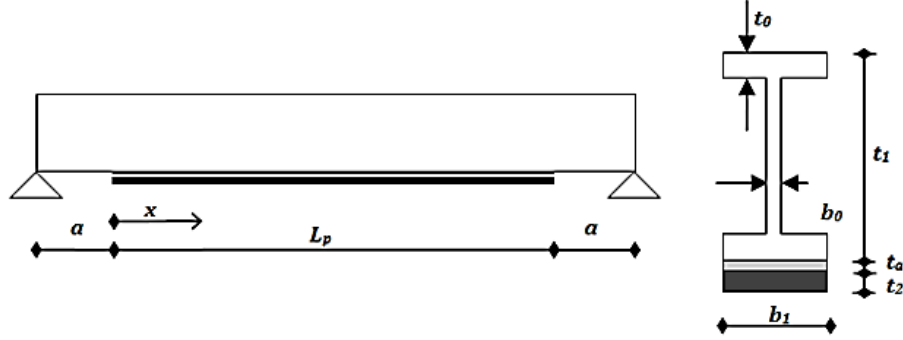
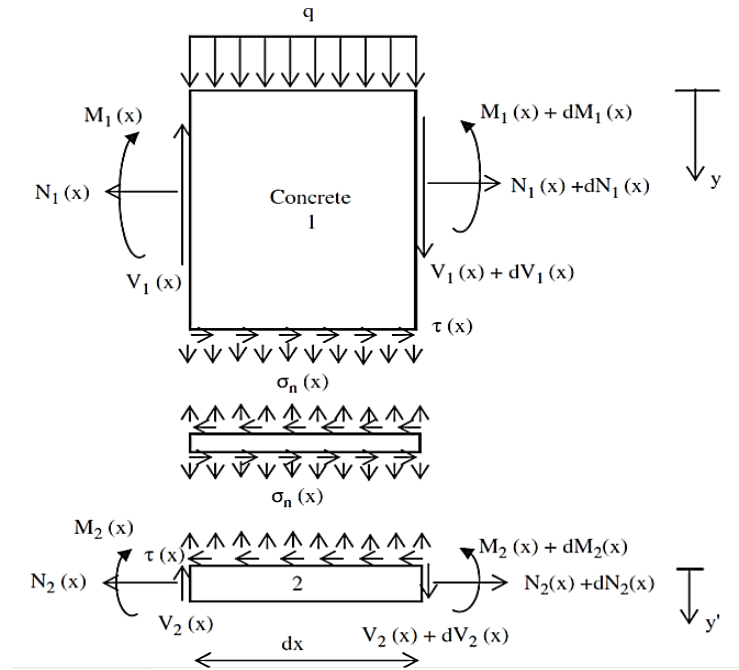Fig. 1 Simply supported beam strengthened with bonded FRP plate

Fig. 2 Forces in infinitesimal element of a soffit – plated beam

$$\varepsilon_1(x) = \frac{du_1(x)}{dx} = \varepsilon_1^M(x) + \varepsilon_1^N(x) + \alpha_1 \Delta T \tag{1}$$

$$\varepsilon_2(x) = \frac{du_2(x)}{dx} = \varepsilon_2^M(x) + \varepsilon_2^N(x) + \alpha_2 \Delta T \tag{2}$$

where, α_1 and α_2 are the thermal expansion coefficients of adherends 1 and 2, respectively. ΔT is the temperature change. $u_1(x)$ and $u_2(x)$ are the longitudinal displacements at the base of adherend 1 and the top of adherend 2, respectively. $\varepsilon_1^M(x)$ and $\varepsilon_2^M(x)$ are the strains induced by the bending moment at adherends 1 and 2, respectively and they are written as follows

$$\varepsilon_1^M(x) = \frac{y_1}{E_1 I_1} M_1(x), \quad \varepsilon_2^M(x) = \frac{y_2}{E_2 I_2} M_2(x) \tag{3}$$

where E is the elastic modulus and I the second moment of area. The subscripts 1 and 2 denote adherends 1 and 2, respectively. $M(x)$ is the bending moment while y_1 and y_2 are the distances from the bottom of adherend 1 and the top of adherend 2 to their respective centroid. $\varepsilon_1^N(x)$ and $\varepsilon_2^N(x)$ are the unknown longitudinal strains of the beam and FRP reinforcement, respectively, at the adhesive interface and they are due to the longitudinal forces. These strains are given as follows

$$\varepsilon_1^N(x) = \frac{du_1^N(x)}{dx}, \quad \varepsilon_2^N(x) = \frac{du_2^N(x)}{dx} \tag{4}$$

where $u_1^N(x)$ and $u_2^N(x)$ represents the longitudinal force-induced adhesive displacement at the interface between the upper (lower) adherend and the adhesive.

To determine the unknown longitudinal strains $\varepsilon_1^N(x)$ and $\varepsilon_2^N(x)$, shear deformations of the adherends are incorporated in this analysis. It is reasonable to assume that the shear stresses, which develop in the adhesive, are continuous across the adhesive-adherend interface. In addition, equilibrium requires the shear stress to be zero at the free surface. Using the same methodology developed by Tsai *et al.* (1998) and Tounsi (2006), this effect is taken into account. A cubic variation of longitudinal displacements $U_1^N(x, y)$ and $U_1^N(x, y)$ in both adherends is assumed

$$U_1^N(x, y) = A_1(x)y^3 + B_1(x)y + C_1(x) \tag{5}$$

$$U_2^N(x, y) = A_2(x)y^3 + B_2(x)y + C_2(x) \tag{6}$$

where $y(y')$ is a local coordinate system with the origin at the top surface of the upper (lower) adherend (Fig. 2).

The shear stresses in the two adherends are given by

$$\sigma_{xy(1)} = G_1 \gamma_{xy(1)} \tag{7}$$

$$\sigma_{xy(2)} = G_2 \gamma_{xy(2)} \tag{8}$$

G_1 and G_2 are the transverse shear moduli of adherends 1 and 2, respectively. Neglecting the variations of transverse displacement W_i^N (induced by the longitudinal forces) with the longitudinal coordinate x

$$\gamma_{xy(i)} \approx \frac{\partial U_i^N}{\partial y} \tag{9}$$

The shear stresses are given by

$$\sigma_{xy(1)} = G_1 \left[3A_1(x)y^2 + B_1(x) \right] \tag{10}$$

$$\sigma_{xy'(2)} = G_2 \left[3A_2(x)y'^2 + B_2(x) \right] \tag{11}$$

The shear stresses must satisfy the following conditions

$$\sigma_{xy(1)}(x,t_1) = \sigma_{xy'(2)}(x,0) = \tau(x) = \tau_a \tag{12}$$

$$\sigma_{xy(1)}(x,0) = 0, \quad \sigma_{xy'(2)}(x,t_2) = 0 \tag{13}$$

where t_1 and t_2 are the thickness of adherends 1 and 2, respectively.

Condition Eq. (12) follows from continuity and assumption of uniform shear stresses ($\tau(x) = \tau_a$) through the thickness of adhesive. Condition (Eq. (13)) states there is no shear stress at the top surface of the adherend 1 (i.e., at $y = 0$) and the bottom surface of adherend 2 (i.e., at $y' = 0$). These conditions yield

$$\sigma_{xy(1)} = \frac{\tau_a}{t_1^2} y^2 \tag{14}$$

$$\sigma_{xy'(2)} = \left(1 - \frac{y'^2}{t_2^2}\right)\tau_a \tag{15}$$

Then, with a linear material constitutive relationship, the adherend shear strain γ_1 for adherend 1 and γ_2 for adherend 2 are written as

$$\gamma_{xy(1)} = \gamma_1 = \frac{\tau_a}{G_1 t_1^2} y^2 \tag{16}$$

$$\gamma_{xy'(2)} = \gamma_2 = \frac{\tau_a}{G_2}\left(1 - \frac{y'^2}{t_2^2}\right) \tag{17}$$

The longitudinal displacement functions U_1^N for the upper adherend and U_2^N for the lower adherend, due to the longitudinal forces, are given as

$$U_1^N(y) = U_1^N(0) + \int_0^y \gamma_1(y)dy = U_1^N(0) + \frac{\tau_a}{3G_1 t_1^2} y^3 \tag{18}$$

$$U_2^N(y) = u_2^N(0) + \int_0^{y'} \gamma_2(y')dy' = u_2^N(0) + \frac{\tau_a}{G_2}\left(y' - \frac{y'^3}{3t_2^2}\right) \tag{19}$$

where $U_1^N(0)$ represents the displacement at the top surface of the upper adherend (due to the longitudinal forces) and u_2^N is the longitudinal force-induced adhesive displacement at the interface between the adhesive and lower adherend.

Note that due to the perfect bonding of the joints, the displacements are continuous at the interfaces between the adhesive and adherends. As a result, u_2^N should be equivalent to the lower adherend displacement at the interface and u_1^N (the adhesive displacement at the interface between the adhesive and upper adherend) should be the same as the upper adherend displacement at the interface. Based on Eq. (18), u_1^N can be expressed as

$$u_1^N = U_1^N(y = t_1) = U_1^N(0) + \frac{\tau_a t_1}{3G_1} \tag{20}$$

Using Eq. (20), Eq. (18) can be rewritten as

$$U_1^N(y) = u_1^N + \frac{\tau_a}{3G_1 t_1^2} y^3 - \frac{\tau_a t_1}{3G_1} \tag{21}$$

The longitudinal resultant forces, N_1 and N_2, for the upper and lower adherends, respectively, are

$$N_1 = b_1 \int_0^{t_0} \sigma_1^N(y)dy + b_0 \int_{t_0}^{t_1-t_0} \sigma_1^N(y)dy + b_1 \int_{t_1-t_0}^{t_1} \sigma_1^N(y)dy \tag{22}$$

$$N_2 = b_2 \int_0^{t_2} \sigma_2^N(y')dy' \tag{23}$$

where σ_1^N and σ_2^N are longitudinal normal stresses for the upper and lower adherends, respectively. By changing these stresses into functions of displacements and substituting Eqs. (19) and (21) into the displacements, Eqs. (22) and (23) can be rewritten as

$$\begin{aligned} N_1 &= E_1 b_1 \int_0^{t_1} \frac{dU_1^N}{dx}dy + E_1 b_0 \int_{t_0}^{t_1-t_0} \frac{dU_1^N}{dx}dy + E_1 b_1 \int_{t_1-t_0}^{t_1} \frac{dU_1^N}{dx}dy \\ &= E_1 A_1 \frac{du_1^N(x)}{dx} - \frac{E_1}{t_1 G_1}\left[\frac{1}{3}t_0(2t_1 - t_0)\left(\frac{1}{2}t_1 + t_0\right)(b_1 - b_0) + \frac{1}{4}b_0 t_1^3\right]\frac{d\tau_a(x)}{dx} \end{aligned} \tag{24}$$

and

$$N_2 = E_2 b_2 \int_0^{t_2} \frac{dU_2^N}{dx}dy' = E_2 A_2 \left(\frac{du_2^N}{dx} + \frac{5t_2}{12G_2}\frac{d\tau_a}{dx}\right) \tag{25}$$

Hence, the longitudinal strains induced by the longitudinal forces (Eq. (4)) can be written as

$$\varepsilon_1^N(x) = \frac{du_1^N(x)}{dx} = \frac{N_1}{E_1 A_1} + \frac{1}{t_1 G_1 A_1}\left[\frac{1}{3}t_0(2t_1 - t_0)\left(\frac{1}{2}t_1 + t_0\right)(b_1 - b_0) + \frac{1}{4}b_0 t_1^3\right]\frac{d\tau_a(x)}{dx} \tag{26}$$

$$\varepsilon_2^N(x) = \frac{du_2^N(x)}{dx} = \frac{N_2}{E_2 A_2} - \frac{5t_2}{12G_2}\frac{d\tau_a(x)}{dx} \tag{27}$$

Substituting Eqs. (26), (27) and (3) into Eqs. (1) and (2), respectively, these latter become

$$\varepsilon_1(x) = \frac{du_1(x)}{dx} = \frac{y_1}{E_1 I_1} M_1(x) + \frac{N_1(x)}{E_1 A_1}$$
$$+ \frac{1}{t_1 G_1 A_1} \left[\frac{1}{3} t_0 (2t_1 - t_0) \left(\frac{1}{2} t_1 + t_0 \right)(b_1 - b_0) + \frac{1}{4} b_0 t_1^3 \right] \frac{d\tau(x)}{dx} + \alpha_1 \Delta T \tag{28}$$

$$\varepsilon_2(x) = \frac{du_2(x)}{dx} = \frac{-y_2}{E_2 I_2} M_2(x) + \frac{N_2(x)}{E_2 A_2} - \frac{5t_2}{12 G_2} \frac{d\tau(x)}{dx} + \alpha_2 \Delta T \tag{29}$$

where $N(x)$ is the axial force in each adherend and A is the cross-sectional area.

The shear stress in the adhesive can be expressed as follows

$$\tau_a = \tau(x) = K_S \left[u_2(x) - u_1(x) \right] \tag{30}$$

where $K_s = G_a / t_a$ is shear stiffness of the adhesive; G_a and t_a are shear modulus and thickness of the adhesive, respectively, and $u_1(x)$ and $u_2(x)$ are the longitudinal displacements at the base of adherend 1 and the top of adherend 2. Differentiating the above expression we obtain

$$\frac{d\tau(x)}{dx} = K_S \left[\frac{du_2(x)}{dx} - \frac{du_1(x)}{dx} \right] \tag{31}$$

Consideration of horizontal equilibrium gives

$$\frac{dN_1(x)}{dx} = -b_2 \tau(x) \tag{32}$$

$$\frac{dN_2(x)}{dx} = b_2 \tau(x) \tag{33}$$

where

$$N_2(x) = N(x) = b_2 \int_0^x \tau(x) dx \tag{34}$$

$$N_1(x) = -N(x) = -b_2 \int_0^x \tau(x) dx \tag{35}$$

and b_2 is the width of the FRP plate.

Assuming equal curvature in the beam and the FRP plate, the relationship between the moments in the two adherends can be expressed as

$$M_1(x) = RM_2(x) \tag{36}$$

with

$$R = \frac{E_1 I_1}{E_2 I_2} \tag{37}$$

Moment equilibrium of the differential segment of the plated beam in Fig. 2 gives

$$M_T(x) = M_1(x) + M_2(x) + N(x)[y_1 + y_2 + t_a] \tag{38}$$

where $M_T(x)$ is the total applied moment.

The bending moment in each adherend, expressed as a function of the total applied moment and the interfacial shear stress, is given as

$$M_1(x) = \frac{R}{R+1}\left[M_T(x) - b_2 \int_0^x (y_1 + y_2 + t_a)\tau(x)dx \right] \tag{39}$$

$$M_2(x) = \frac{1}{R+1}\left[M_T(x) - b_2 \int_0^x (y_1 + y_2 + t_a)\tau(x)dx \right] \tag{40}$$

The first derivative of the bending moment in each adherend gives

$$\frac{dM_1(x)}{dx} = \frac{R}{R+1}\left[V_T(x) - b_2\tau(x)(y_1 + y_2 + t_a) \right] \tag{41}$$

$$\frac{dM_2(x)}{dx} = \frac{1}{R+1}\left[V_T(x) - b_2\tau(x)(y_1 + y_2 + t_a) \right] \tag{42}$$

Substituting Eqs. (28) and (29) into Eq. (31) and differentiating the resulting equation yields

$$\frac{d^2\tau(x)}{dx^2} = K_S\left(\frac{1}{E_2 A_2}\frac{dN_2(x)}{dx} - \frac{y_2}{E_2 I_2}\frac{dM_2(x)}{dx} - \frac{y_1}{E_1 I_1}\frac{dM_1(x)}{dx} - \frac{1}{E_1 A_1}\frac{dN_1(x)}{dx} \right)$$
$$- K_S\left[\frac{5t_2}{12G_2} + \frac{1}{t_1 G_1 A_1}\left(\frac{1}{3}t_0(2t_1 - t_0)(b_1 - b_0) + \frac{1}{4}b_0 t_1^3 \right) \right]\frac{d^2\tau(x)}{dx^2} \tag{43}$$

Substitution of the shear forces (Eqs. (41) and (42)) and axial forces (Eqs. (34) and (35)) into Eq. (43) gives the following governing differential equation for the interfacial shear stress

$$\frac{d^2\tau(x)}{dx^2} - K_1 b_2\left(\frac{(y_1 + y_1)(y_1 + y_1 + t_a)}{E_1 I_1 + E_2 I_2} + \frac{1}{E_1 A_1} + \frac{1}{E_2 A_2} \right)\tau(x) + K_1\left(\frac{y_1 + y_2}{E_1 I_1 + E_2 I_2} \right)V_T(x) = 0 \tag{44}$$

where

$$K_1 = \frac{1}{\left(\dfrac{t_a}{G_a} + \dfrac{t_1}{4G_1}\xi + \dfrac{5t_2}{12G_2} \right)} \tag{45}$$

and ξ is a geometrical coefficient which is given as

$$\xi = \frac{1}{t_1^2 A_1}\left(\frac{4}{3}t_0(2t_1 - t_0)\left(\frac{1}{2}t_1 + t_0\right)(b_1 - b_0) + b_0 t_1^3\right)$$

(46)

For a rectangular section ($b_1 = b_0$), $\xi = 1$ which corresponds to the same expression given by Tounsi *et al.* (2009) by neglecting shear deformations of the FRP plate. However, for I-beam section we have $\xi < 1$.

2.3 Normal stress distribution along the FRP-beam interface

The interfacial normal stress in the adhesive can be expressed as follows

$$\sigma_n(x) = K_n \Delta w(x) = K_n \left[w_2(x) - w_1(x)\right]$$

(47)

where K_n is the normal stiffness of the adhesive per unit length and can be written as

$$K_n = \frac{\sigma_n(x)}{\Delta w(x)} = \frac{\sigma_n(x)}{\Delta w(x)/t_a}\left(\frac{1}{t_a}\right) = \frac{E_a}{t_a}$$

(48)

and $w_1(x)$ and $w_2(x)$ are the normal displacement of adherends 1 and 2, respectively.

Differentiating Eq. (47) twice results in

$$\frac{d^2\sigma_n(x)}{dx^2} = K_n\left[\frac{d^2 w_2(x)}{dx^2} - \frac{d^2 w_1(x)}{dx^2}\right]$$

(49)

Considering the moment-curvature relationships for the beam and the external reinforcement, respectively, gives

$$\frac{d^2 w_1(x)}{dx^2} = \frac{M_1(x)}{E_1 I_1} \quad \text{and} \quad \frac{d^2 w_2(x)}{dx^2} = -\frac{M_2(x)}{E_2 I_2}$$

(50)

The equilibrium of adherends 1 and 2, leads to the following relationships:
Adherend 1:

$$\frac{dM_1(x)}{dx} = V_1(x) - b_2 y_1 \tau(x) \quad \text{and} \quad \frac{dV_1(x)}{dx} = -b_2\sigma_n(x) - q$$

(51)

Adherend 2:

$$\frac{dM_2(x)}{dx} = V_2(x) - b_2 y_1 \tau(x) \quad \text{and} \quad \frac{dV_2(x)}{dx} = b_2\sigma_n(x)$$

(52)

Based on the above equilibrium equations, the governing differential equations for the deflection of the adherends 1 and 2, expressed in terms of the interfacial shear and normal stresses, are given as follows:

Adherend 1

$$\frac{d^4 w_1(x)}{dx^4} = \frac{1}{E_1 I_1} b_2 \sigma_n(x) + \frac{y_1}{E_1 I_1} b_2 \frac{d\tau(x)}{dx} + \frac{q}{E_1 I_1} \tag{53}$$

Adherend 2

$$\frac{d^4 w_2(x)}{dx^4} = \frac{-1}{E_2 I_2} b_2 \sigma_n(x) + \frac{y_2}{E_2 I_2} b_2 \frac{d\tau(x)}{dx} \tag{54}$$

Substitution of Eqs. (53) and (54) into the fourth derivation of the interfacial normal stress obtainable from Eq. (47) gives the following governing differential equation for the interfacial normal stress

$$\frac{d^4 \sigma_n(x)}{dx^4} + \frac{E_a b_2}{t_a} \left(\frac{1}{E_1 I_1} + \frac{1}{E_2 I_2} \right) \sigma_n(x) + \frac{E_a b_2}{t_a} \left(\frac{y_1}{E_1 I_1} - \frac{y_2}{E_2 I_2} \right) \frac{d\tau(x)}{dx} + \frac{q E_a}{t_a E_1 I_1} = 0 \tag{55}$$

2.4 Finite difference solution

The governing differential equations for shear stress (Eq. (44)) and normal stress (Eq. (55)) are valid for plated beams with geometric and material properties that are constant along its length. However, in case of complex plate-end geometry (taper) a closed form solution is not possible. A finite difference method (FDM) can be used to evaluate the adhesive stresses for cases with varying section properties.

A finite difference solution using constant node spacing, h, is outlined below. The nodes are numbered with real nodes from $x = 0$ to $x = L/2$, in addition to virtual nodes $(1, 2, n+3, n+4)$ which are used to allow derivatives to be defined at nodes 3 and $n+2$. Subscripts are used to define nodes' numbers in the following equations. According to Fig. 3, the finite difference solution shows a good convergence for shear and normal stresses, thus, in order to obtain accurate results, a fine mesh of 2000 nodes has been used for all analysis.
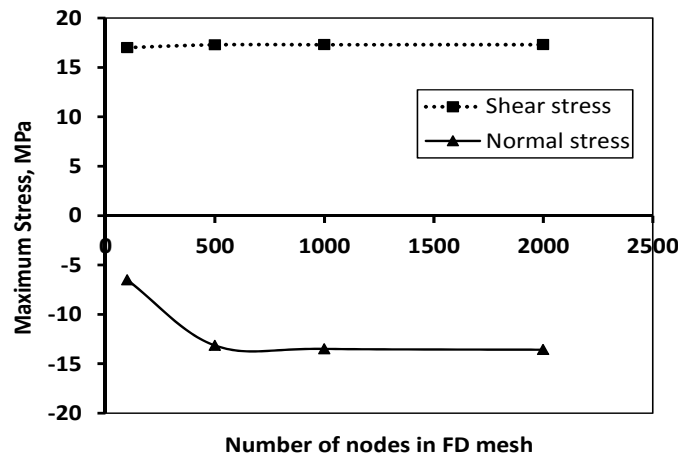

Fig. 3 Convergence of Finite difference solution

2.4.1 Interfacial shear stress

The governing differential equation (Eq. (44)) for the interfacial shear stress is simplified as

$$\frac{d^2\tau}{dx^2} + f_1\frac{d\tau}{dx} = f_2 V(x) \tag{56}$$

where

$$f_1 = -K_1 b_2\left(\frac{(y_1 + y_2)(y_1 + y_2 + t_a)}{E_1 I_1 + E_2 I_2} + \frac{1}{E_1 A_1} + \frac{1}{E_2 A_2}\right) \tag{57}$$

$$f_2 = -K_1\left(\frac{y_1 + y_2}{E_1 I_1 + E_2 I_2}\right) \tag{58}$$

The Eq. (56) can be written in finite difference format as

$$\frac{\tau_{i-1} - 2\tau_i + \tau_{i+1}}{h^2} + f_1\tau_i = f_2 V(x), \quad i = 3.....(n+2) \tag{59}$$

Considering the following boundary conditions:
(1) Due to symmetry the shear stress at mid-span is zero

$$\tau\left(\frac{L}{2}\right) = \tau_{n+2} = 0 \tag{60}$$

(2) At the end of FRP plate, the longitudinal force $N_1(0) = N_2(0)$ and the moment $M_2(0)$ are zero. As a result, the moment in the section at the plate curtailment is resisted by the beam alone. Thus

$$M_1(0) = M_T(0) = \frac{qa}{2}(L - a) \tag{61}$$

Using this boundary condition in Eq. (31)

$$\frac{d\tau(x=0)}{dx} - K_1\left(\frac{y_1}{E_1 I_1}M_T(0) + (\alpha_1 - \alpha_2)\Delta T\right) \tag{62}$$

Eq. (62) can be written as

$$\frac{-\tau_2 + \tau_4}{2h} = -K_1\left(\frac{y_1}{E_1 I_1}M_T(0) + (\alpha_1 - \alpha_2)\Delta T\right) \tag{63}$$

By writing Eq. (59) at the plate-end (node 3) and eliminating τ_2 using Eq. (63), we get

$$\left(h^2 f_1 - 2\right)\tau_3 + 2\tau_4 = h^2 f_2 - 2hK_1\left(\frac{y_1}{E_1 I_1}M_T(0) + (\alpha_1 - \alpha_2)\Delta T\right) \tag{64}$$

Finally, by combining Eqs. (59), (60), and (64) gives

$$
\begin{bmatrix}
(f_1 h^2 - 2) & 2 & & & & \\
 & 1 & (f_1 h^2 - 2) & 1 & & \\
 & & & \ddots & & \\
 & & & 1 & (f_1 h^2 - 2) & 1 \\
 & & & & & 1
\end{bmatrix}
\begin{Bmatrix}
\tau_2 \\
\tau_4 \\
\vdots \\
\tau_{n-1} \\
\tau_{n-2}
\end{Bmatrix}
$$

$$
= \begin{Bmatrix}
h^2 f_2 - 2hK_1 \left(\dfrac{y_1}{E_1 I_1} M_T(0) + (\alpha_1 - \alpha_2)\Delta T \right) \\
f_2 h^2 V(x) \\
\vdots \\
f_2 h^2 V(x) \\
0
\end{Bmatrix}
\tag{65}
$$

These n simultaneous equations are solved explicitly to find the plate force at each of the n nodes.

2.4.2 Interfacial normal stress

A fourth order finite – difference solution is required to find the normal shear stress. The governing equation for normal stress (Eq. (55)) is written at each node ($i = 3 \ldots n + 2$) along the beam

$$
\frac{d^4 \sigma(x)}{dx^4} + g_1 \sigma(x) = g_2 \frac{d\tau(x)}{dx} + g_3
\tag{66}
$$

where

$$
g_1 = \frac{E_a b_2}{t_a} \left(\frac{1}{E_1 I_1} + \frac{1}{E_2 I_2} \right)
\tag{67}
$$

$$
g_2 = -\frac{E_a b_2}{t_a} \left(\frac{y_1}{E_1 I_1} - \frac{y_2}{E_2 I_2} \right)
\tag{68}
$$

$$
g_3 = -\frac{q E_a}{t_a E_1 I_1}
\tag{69}
$$

Eq. (66) can be written in finite difference at i^{th} node as

$$
\frac{\sigma_{i-2} - 4\sigma_{i-1} + 6\sigma_i - 4\sigma_{i+1} + \sigma_{i+2}}{h^4} + g_1 \sigma_i = g_2 \frac{d\tau(x)}{dx} + g_3, \quad i = 3, \ldots n + 2
\tag{70}
$$

Considering the following boundary conditions:
(1) At center the normal stress is zero

$$\sigma(x = L/2) = \sigma_{n+2} = 0 \tag{71}$$

(2) At the plate ends, the bending moment equals to zero. By Substituting Eq. (50) into Eq. (49) and expressing the result at the plate-end (x=0) yields

$$\left.\frac{d^2\sigma(x)}{dx^2}\right|_{x=0} = \frac{E_a}{t_a}\left(\frac{M_1(0)}{E_1 I_1} - \frac{M_2(0)}{E_2 I_2}\right) \tag{72}$$

The boundary condition leads to $M_2(0) = 0$ and $M_1(0) = M_T(0)$. Thus Eq. (72) can be expressed as

$$\left.\frac{d^2\sigma(x)}{dx^2}\right|_{x=0} = \frac{E_a}{t_a}\frac{M_T(0)}{E_1 I_1} \tag{73}$$

Using the finite difference format the above equation becomes

$$\frac{\sigma_2 - 2\sigma_3 + \sigma_4}{h^2} = \frac{E_a}{t_a}\frac{M_T(0)}{E_1 I_1} \tag{74}$$

(3) The shear force at the plate ends equals to zero. Differentiating Eq. (49) and substituting Eqs. (51) and (52) into the resulting which may be expressed at the plate-end as follows

$$\left.\frac{d^3\sigma(x)}{dx^3}\right|_{x=0} = \frac{E_a}{t_a}\left(\frac{V_1(0)}{E_1 I_1} - \frac{V_2(0)}{E_2 I_2}\right) - \frac{E_a b_2}{t_a}\left(\frac{y_1}{E_1 I_1} - \frac{y_2}{E_2 I_2}\right)\tau(0) \tag{75}$$

The boundary condition leads to $V_2(0) = 0$ and $V_1(0) = V_T(0)$. Thus Eq. (75) can be expressed as

$$\left.\frac{d^3\sigma(x)}{dx^3}\right|_{x=0} = \frac{E_a}{t_a}\frac{V_T(0)}{E_1 I_1} + g_2\tau(0) \tag{76}$$

which can be expressed in finite difference format as

$$\frac{-\sigma_1 + 2\sigma_2 - 2\sigma_4 + \sigma_5}{2h^3} = \frac{E_a}{t_a}\frac{V_T(0)}{E_1 I_1} + g_2\tau(0) \tag{77}$$

Eq. (70) can be written at node 3 after eliminating σ_1 and σ_2 using Eqs. (74) and (77) as follows

$$\sigma_3\left(2 + h^4 g_1\right) - 4\sigma_4 + 2\sigma_5 = h^4\left(g_2\frac{d\tau(x)}{dx} + g_3\right) + 2h^3\left(\frac{E_a}{t_a}\frac{V_T(0)}{E_1 I_1} + g_2\tau(0)\right) + 2h^2\frac{E_a}{t_a}\frac{M_T(0)}{E_1 I_1} \tag{78}$$

Also, at node 4, Eq. (70) can be written after eliminating σ_2 using Eq. (74) as

$$-2\sigma_3 + \sigma_4\left(5 + h^4 g_1\right) - 4\sigma_5 + \sigma_6 = h^4\left(g_2\frac{d\tau(x)}{dx} + g_3\right) - h^2\frac{E_a}{t_a}\frac{M_T(0)}{E_1 I_1} \tag{79}$$

Finally, combining Eqs. (71), (78), and (79) yields a system of *n* simultaneous equations as follows

$$
\begin{bmatrix}
(2 + h^4 g_1) & -4 & 2 \\
-2 & (5 + h^4 g_1) & -4 & -1 \\
1 & -4 & (6 + h^4 g_2) & -4 & 1 \\
& & & \ddots \\
& & & 1 & -4 & (6 + h^4 g_2) & -4 & 1 \\
& & & & 1 & -4 & (6 + h^4 g_2) & -4 \\
& & & & & & & 1
\end{bmatrix}
\begin{Bmatrix}
\sigma_3 \\
\sigma_4 \\
\sigma_5 \\
\vdots \\
\sigma_n \\
\sigma_{n+1} \\
\sigma_{n+2}
\end{Bmatrix}
$$

$$
=
\begin{Bmatrix}
h^4\left(g_2\dfrac{d\tau(x)}{dx} + g_3\right) + 2h^3\left(\dfrac{E_a}{t_a}\dfrac{V_T(0)}{E_1 l_1} + g_2\tau(0)\right) + 2h^2\dfrac{E_a}{t_a}\dfrac{M_T(0)}{E_1 l_1} \\
h^4\left(g_2\dfrac{d\tau(x)}{dx} + g_3\right) - h^2\dfrac{E_a}{t_a}\dfrac{M_T(0)}{E_1 l_1} \\
\vdots \\
g_2\dfrac{d\tau(x)}{dx} + g_3 \\
g_2\dfrac{d\tau(x)}{dx} + g_3 \\
0
\end{Bmatrix}
\tag{80}
$$

These *n* simultaneous equations are solved explicitly for normal stress at each of the *n* nodes. The normal stress distribution follows.

3. Results and discussion

3.1 FRP Plate with constant thickness

Comparison of the results
An I-section steel beam which was carried out by Deng *et al*. (2004) is used for comparison with present method since the effect of transverse shear has been included in addition to shear correction factor (ξ). The span of the I-section beam is 5000 m, the distance from the support to the end of the plate is 500 mm. the beam is subjected to thermal loading of $\Delta T = 50°C$. The cross section properties of I-beam and the material properties are listed in Table 1.

According to 2 and Fig. 4 it is noted that the results of the present method show a lower maximum stresses compared to results obtained by Deng *et al*. (2004). Therefore, the inclusion of shear deformation effect decreases the interfacial maximum stresses, noting that the present

Table 1 Dimensions and material properties of the I-section composite beam

Component	Width b, [mm]	Depth t, [mm]	Young's modulus E, [GPa]	Poisson's ratio	Shear modulus G, [Gpa]
Beam	$b_0 = 211.9$ $b_1 = 12.7$	$t_0 = 544.5$ $t_1 = 21.3$	210	0.3	-
Adhesive layer	211.9	2	10	0.3	3.7
FRP plate	211.9	12	310	0.3	3.7

Table 2 comparison of maximum interfacial stresses for the I-section beam

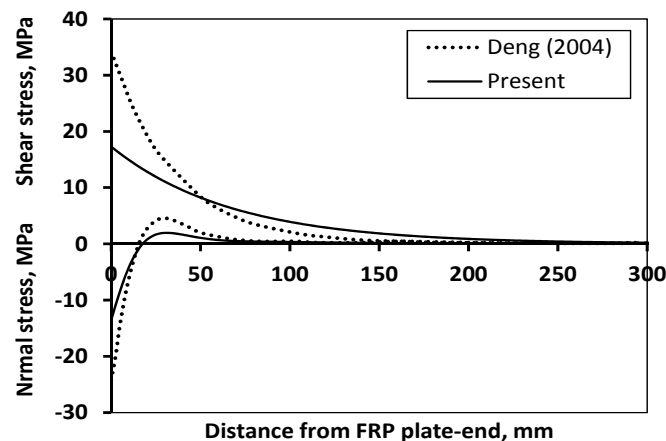|	Thermal loading $\Delta T = 50°C$	
	Shear stress (MPa)	Normal stress(MPa)
Deng *et al*. (2004)	34.50	25.60
Present FDM	17.31	13.58

Fig. 4 Comparaison of interfacial normal and shear stresses forFRP-plated I-section steel beam

method takes into account a parabolic shear distribution while Deng *et al*. (2004) method has not included the shear deformation effect. This later phenomenon has been already confirmed by Tounsi *et al*. (2009) and Belakhdar *et al*. (2011) for beams under mechanical loading.

Effect of FRP plate thickness

The thickness of the FRP plate is an important design variable in practice. Fig. 5 shows the effect of the thickness of the FRP plate on the maximum interfacial stresses. It is shown that the level and concentration of interfacial stress are influenced considerably by the thickness of the FRP plate. The interfacial stresses increase as the thickness of FRP plate increases. Noting that, in the practice, FRP plates have generally a small thickness compared to that of steel plates. Therefore, in terms of stress concentration due to plate thickness, the use of FRP plates is more advantageous than the use of steel plates.
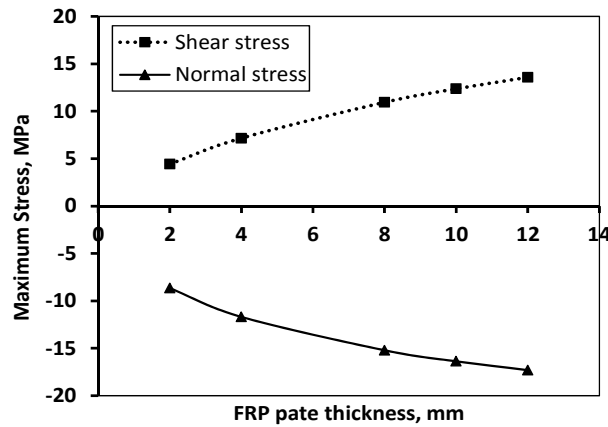
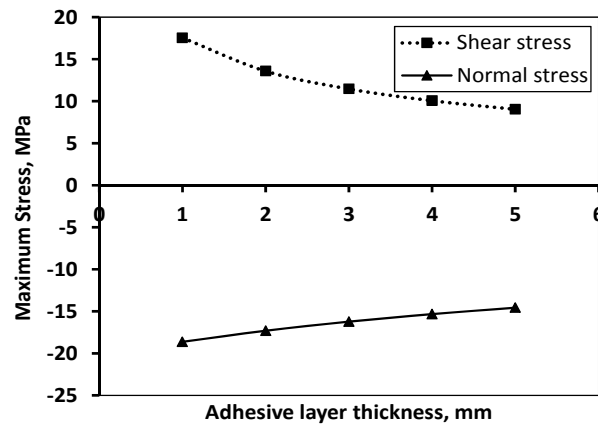Fig. 5 Effect of FRP plate thickness on the maximum interfacial stresses

Fig. 6 Effect of adhesive layer thickness on the maximum interfacial stresses

Effect of adhesive layer thickness

The effect of adhesive layer thickness is shown in Fig. 6. It is noted that as the thickness of the adhesive layer increases, the maximum shear and normal stress decrease. This relation between adhesive layer thickness and the maximum stresses is expected since the adhesive layer is relatively soft and has a smaller stiffness, in addition to the fact that as the thickness increases, the layer become more softer which reduces the stress concentration in the layer.

3.2 FRP Plate with taper

Effect of taper shape

Herein the effect of FRP plate with a generally variable thickness is presented. The thickness of the FRP plate $t_2 = t_2(x)$ is described by arbitrary function of the longitudinal coordinate x; hence the cross-sectional area and the second moment of area of the FRP plate, $A_2(x)$ and $I_2(x)$, are also functions of the coordinate x. three particular cases are examined as shown in Fig. 7. Noting that in this parametric study, the I-section steel beam is chosen to be studied where its geometric and
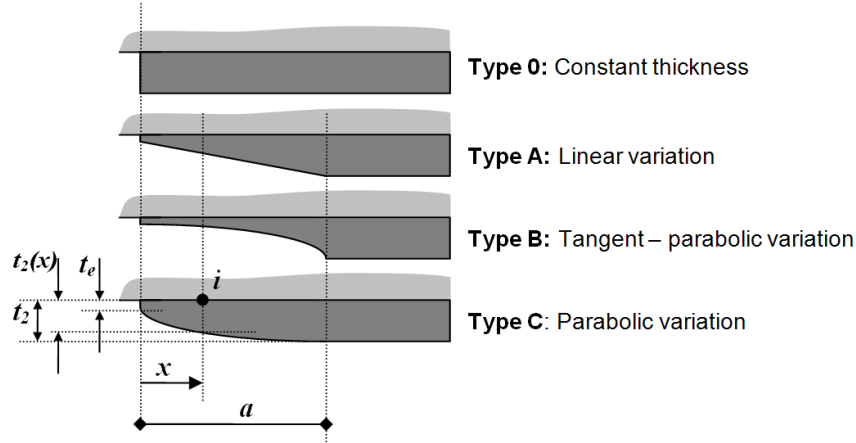
Fig. 7 Taper patterns of FRP plate

materials properties are kept fixed. Thus, only the taper geometric properties are studied according to the following patterns:

Type 0: constant variation

$$t_2(x) = t_2 \tag{81}$$

Type A: linear variation

$$t_2(x) = \begin{cases} \dfrac{t_2 - t_e}{a} x + t_e & \text{for} \quad 0 \leq x \leq a \\[2ex] t_2 & \text{for} \quad a \leq x \leq \dfrac{L}{2} \end{cases} \tag{82}$$

Type B: Tangent – parabolic variation

$$t_2(x) = \begin{cases} \dfrac{t_2 - t_e}{a^2} x^2 + t_e & \text{for} \quad 0 \leq x \leq a \\[2ex] t_2 & \text{for} \quad a \leq x \leq \dfrac{L}{2} \end{cases} \tag{83}$$

Type C: Parabolic variation

$$t_2(x) = \begin{cases} -\dfrac{(t_2 - t_e)}{a^2} x^2 + 2\dfrac{(t_2 - t_e)}{a} x + t_e & \text{for} \quad 0 \leq x \leq a \\[2ex] t_2 & \text{for} \quad a \leq x \leq \dfrac{L}{2} \end{cases} \tag{84}$$

The FRP plate with constant thickness (type 0) will be regarded as the reference case. A numerical study is then conducted to supply information on the contribution of the shape of the thickness profile on the reduction of edge interfacial stresses. In this study, the plated beam is subjected to thermal load of $\Delta T = 50°C$, the length of the taper is $a = 200$ mm and the thickness at

the end of the tape is $t_e = 2$ mm.

From the results presented in Table 3, we can observe that the decrease of the thickness of the FRP plate in the edge region leads to a reduction in the edge stresses. We can also conclude that FRP plate with tangent-parabolic profile i.e., type (B) gives an important reduction in edges interfacial stresses, where a reduction of about 49% and 66% in shear and normal stresses, respectively, is obtained (with respect to the reference case). Fig. 8 describes the typical stress field to clarify the comparison of the results with those of the reference case. Hence, reducing the thickness of the FRP plate in the edge region may be considered as an effective way for reducing the magnitude of the edge stresses involved.

Table 3 Maximum interfacial stresses and percent of reduction in maximum stresses for different taper profiles

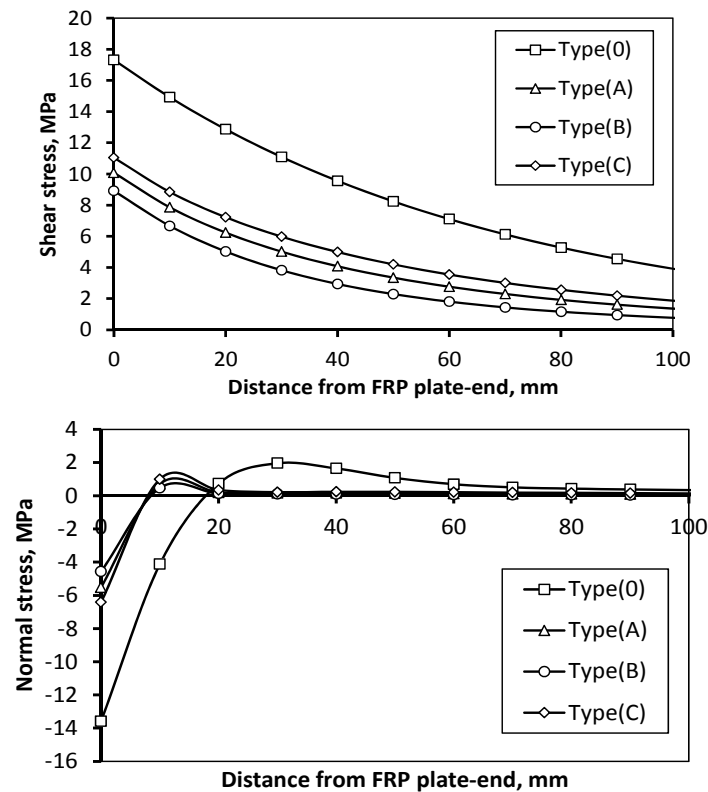|	Max shear stress τ, [MPa]	$\frac{(\tau_{Type(0)} - \tau)}{\tau_{ype(0)}}$ [%]	Max normal stress σ, [MPa]	$\frac{(\sigma_{Type(0)} - \sigma)}{\sigma_{Type(0)}}$ [%]
Type (0)	17.31	-	-13.58	-
Type (A)	10.08	42%	-5.52	59%
Type (B)	8.91	49%	-4.57	66%
Type (C)	11.04	36%	-6.42	53%

Fig. 8 Interfacial stresses for different types of taper profile of FRP plate

Effect of taper profiles geometry

Various parameters influence the maximum values of the shear and normal stresses in the bonding region. In this section of study we used the all types of profiles given in Fig. 7. For retrofitted beams, the most important ones are the thickness and shear modulus of the adhesive, and the thickness and the elastic modulus of the FRP plate. These parameters were studied by several authors (Yang *et al.* 2007, Benyoucef *et al.* 2007, Tounsi *et al.* 2009). In the present study, we intend to show how the maximum interfacial stresses are influenced by the dimension of the taper. The important parameters of the taper are: the length of the taper (*a*) and the thickness at the end of the taper (t_e). Figs. 9 and 10show the maximum interfacial stresses at the tapered end of the plate versus the length of the taper and the thickness end, respectively.

Generally, the parametric study indicates the beneficial effect of having a thin tapered end and a long taper. For the latter, the benefit appears to have saturated when the length of the taper is
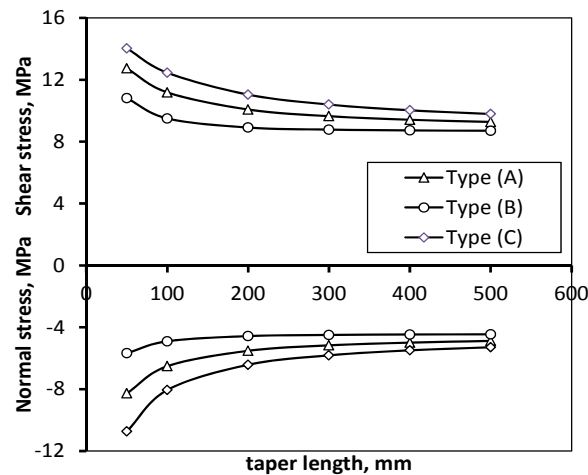

Fig. 9 Maximum interfacial stresses in terms of taper length for different taper profiles
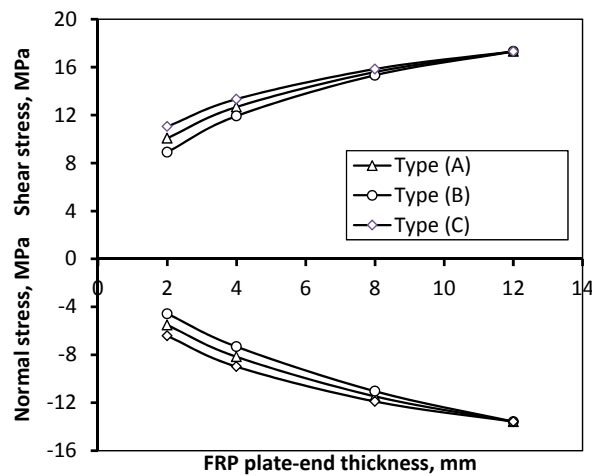

Fig. 10 Maximum interfacial stresses in terms of plate-end thickness for different taper profiles

beyond 400 mm.

According to type of taper, it can be noted that the shape of taper has a sensible effect on maximum interfacial stresses. However it seems that the taper shape has a negligible effect on the maximum stresses when length of the taper (*a*) is grater that 400 mm or the plate-end thickness is greater than 60% of the plate thickness.

4. Conclusions

The present study has developed a relatively simple procedure for evaluating the shear and normal stress concentrations that occur at the edges of the FRP plate in externally strengthened beams under thermal loading. Finite difference method has been employed to solve problems of beams strengthened with plates have complex geometrical extremities.

High stress concentrations occur at the free ends of adhesively bonded plates. Using the tapered edges, however, reduce the maximum shear stresses by at least 15% the maximum stresses. In addition, it has been shown that the shape of the taper has an important effect on the reduction of such stresses, where tangent parabolic stepped taper can reduce better the maximum stresses compared to other taper shapes, where a reduction of about 49% and 66% in shear and normal stresses, respectively, is obtained. Hence, the taper is very beneficial for avoiding debonding of the FRP plates from the beams as long as the taper length is less that 400 mm and the plate-end thickness is less than 60% of the FRP-plate thickness.

The dimensions of the taper also have an influence on the interfacial edge stresses. The maximum shear and normal stresses decrease as the thickness of the end of the taper decreases and the length of the taper increases. However, there is no further change in stress if the length of the taper is increased beyond 400 mm.

References

Arslan, G., Sevuk, F. and Ekiz, I. (2008), "Steel plate contribution to load-carrying capacity of retrofitted RC beams", *Constr. Build. Mater.*, **22**(3), 143-153.

Belakhdar, K., Tounsi, A., Benyoucef, S., Adda-Bedia E.A. and El Hassar, S.M. (2010), "On the reduction of the interfacial stresses in a repaired beam with an adhesively bonded frp plate", *Compos. Interfaces*, **17**(1), 1-14.

Belakhdar, K., Tounsi, A., Adda Bedia, E. and Redha, Y. (2011), "Effect of tapered-end shape of FRP sheets on stress concentration in strengthened beams", *Steel Compos. Struct., Int. J.*, **11**(6), 435-454.

Benyoucef, S., Tounsi, A., Meftah, S.A. and Adda-Bedia, E.A. (2006), "Approximate analysis of the interfacial stress concentrations in FRP–RC hybrid beams", *Compos. Interfaces*, **13**(7), 561-571.

Benyoucef, S., Tounsi, A., Meftah, S.A. and Adda-Bedia, E.A. (2007), "Creep and shrinkage effect on adhesive stresses in RC beams strengthened with composite laminates", *Compos. Sci. Technol.*, **67**(6), 933- 942.

Deng, J., Marcus, M.K.L. and Stuart, S.J.M. (2004), "Stress analysis of steel beams reinforced with a bonded CFRP plate", *Compos. Struct.*, **65**(2), 205-215.

Gao, B., Kim, J.K. and Leung, C.K.Y. (2006a), "Optimization of tapered end design for FRP strips bonded to RC beams", *Compos. Sci. Technol.*, **66**(10), 1266-1273.

Gao, B., Kim, J.K. and Leung, C.K.Y. (2006b), "Strengthening efficiency of taper ended FRP strips bonded to RC beams", *Compos. Sci. Technol.*, **66**(13), 2257-2264.

Gao, B., Kim, J.K. and Leung, C.K.Y. (2006c), "Effect of tapered FRP sheets on interlaminar fracture behaviour of FRP–concrete interface", *Compos. Part A*, **37**(10), 1605-1612.

Hao, S.W., Liu, Y. and Liu, X.D. (2012), "Improved interfacial stress analysis of a plated beam", *Struct. Eng. Mech., Int. J.*, **44**(6), 815-837.

Jones, R., Swamy, R.N. and Charif, A. (1988), "Plate separation and anchorage of reinforced concrete beams strengthened by epoxy bonded steel plates", *Struct. Eng.*, **66**(5), 85-94.

Krour, B., Bernard, F. and Tounsi, A. (2013), "Fibers orientation optimization for concrete beam strengthened with a CFRP bonded plate: A coupled analytical–numerical investigation", *Eng. Struct.*, **56**, 218–227.

Li, G. and Ghebreyesus, A. (2006), "Fast repair of damaged RC beams using UV curing FRP composites", *Compos. Struct.*, **72**(1), 105-110.

Malek, A.M., Saadatmanesh, H. and Ehsani, M.R. (1998), "Prediction of failure load of R/C beams strengthened with FRP plate due to stress concentration at the plate end", *ACI Struct. J.*, **95**(2), 142-152.

Mo, Y.L., Tsai, S.P. and Lee, I.S. (1998), "Seismic performance behaviour of beam – column connections in pre – stressed concrete bridges", *J. Mater. Struct.*, **31**(6), 411-417.

Oehlers, D.J. (1992), "Reinforced concrete beams with plates glued to their soffits", *J. Struct. Eng. ASCE*, **118**(8), 2023-2038.

Panjehpour, M., Farzadnia, N., Anwar, M.P. and Ali, A.A.A. (2011), "FRP sheets contribution in common repair techniques of concrete structures with emphasis on concrete columns", *Int. J. Sustain. Construct. Eng. Technol.*, **2**(2), 54-61.

Pesic, N. and Pilakoutas, K. (2005), "Flexural analysis and design of reinforced concrete beams with externally bonded FRP reinforcement", *Mater. Struct.*, **38**(2), 183-192.

Roberts, T.M. (1989), "Approximate analysis of shear and normal stress concentrations in adhesive layer of plated RC beams", *Struct. Eng.*, **67**(12), 229-233.

Seible, F., Priestley, M.J.N., Hegemier, G.A. and Innamorato, D. (1997), "Seismic retrofit of RC columns with continuous carbon fibre jackets", *J. Comp. Constr.*, **1**(2), 52-62.

Smith, S.T. and Teng, J.G. (2001), "Interfacial stresses in plated RC beams", *Eng. Struct.*, **23**(7), 857-871.

Stratford, T. and Cadei, J. (2006), "Elastic analysis of adhesion stresses for the design of a strengthened plate bonded to a beam", *Constr. Build.Mater.*, **20**(1-2), 34-35.

Swamy, R.N., Jones, R. and Charif, A. (1989), "The effect of external plate reinforcement on the strengthening of structurally damaged RC beams", *Struct. Engr.*, **67**(3), 45-56.

Tounsi, A. (2006), "Improved theoretical solution for interfacial stresses in concrete beams strengthened with FRP plate", *Int. J. Solids Struct.*, **43**(14-15), 4154-4174.

Tounsi, A. and Benyoucef, S. (2007), "Interfacial stresses in externally FRP plated concrete beams", *Int. J. Adhes. Adhes.*, **27**(3), 207-215.

Tounsi, A., Hassaine, T.D., Benyoucef, S. and Adda-Bedia, E.A, (2009), "Interfacial stresses in FRP-plated RC beams: Effect of adherend shear deformations", *Int. J. Adhes. Adhes.*, **29**(4), 343-351.

Tsai, M.Y., Oplinger, D.W. and Morton, J. (1998), "Improved theoretical solutions for adhesive lap joints", *Int. J. Solids Struct.*, **35**(12), 1163-1185.

Yang, J., Ye, J. and Niu, Z. (2007), "Interfacial shear stress in FRP-plated RC beams under symmetric loads", *Cem. Concr. Compos.*, **29**(5), 421-432.

Yang, J., Chen, J.F. and Teng, J.G. (2009), "Interfacial stress analysis of plated beams under symmetric mechanical and thermal loading", *Construct. Build. Mater.*, **23**(9), 2973-2987.

Yang, J. and Ye, J.Q. (2010), "An improved closed-form solution to interfacial stresses in plated beams using a two-stage approach", *Int. J. Mech. Sci.*, **52**(1), 13-30.

Yuan, H. and Lin, Z. (2009), "Theoretical model on interface failure mechanism of reinforced concrete continuous beam strengthened by FRP", *Acta Mech. Solida Sinica*, **22**(2), 161-170.

Zhu, Y. and Zhang, Y.X. (2010), "Nonlinear finite element analyses of FRP-reinforced concrete slabs using a new layered composite plate element", *Comput. Mech.*, **46**(3), 410-430.

CC